AUTOMATED VESSEL DIAMETER MEASUREMENT FROM INTRAVITAL MICROSCOPY

A Thesis

Presented to the Faculty of the Graduate School

of Cornell University

in Partial Fulfillment of the Requirements for the Degree of

Master of Science

by

Jaesung Lee

February 2010

ABSTRACT

Intravital video microscopy is widely used for observing mammalian vasculature *in vivo*. In microcirculation research, the effect of various stimuli on vasculature is often studied using intravital microscopy. The vessel diameter is a commonly reported indicator for such an effect and needs to be accurately measured. Image sequences acquired using intravital microscopy span several minutes in length, and the current practice of manual measurement using electronic calipers or image shearing is time-consuming and prone to measurement error.

Automation of vessel measurement would provide an alternative that is faster and more reliable. The goal of this work was to develop and evaluate an algorithm for automatically measuring the diameter of a vessel from intravital video microscopy data. The proposed method tracks the vessel diameter throughout the entire image sequence once the diameter is marked in the first video frame. Two seed points, indicating the vessel diameter, are placed on the vessel walls and tracked throughout the entire image sequence using feature tracking algorithm. The algorithm parameters were optimized using intravital microscopy image sequences. The ground truth was established manually for each case, and the optimal parameters were found by minimizing deviation from the ground truth.

The accuracy of the method was validated using both synthetic and real intravital image sequences. On synthetic dataset, The automated measurements deviated from the ground truth by an average of 0.0 pixels, while the manual measurement had the average mean squared error of 1.74 pixels. When the ac-

curacy was further evaluated on fluorescence-confocal and non-confocal transmission microscopy image sequences, it was found that the automated method can measure the diameter accurately based on expert visual assessment.

Furthermore, the repeatability of the automated measurements was evaluated based on Bland-Altman analysis and compared to that of the manual measurements. The 95% limits of agreement were found to be [-1.36 μm, 1.52 μm] for the automated method and [-3.08 μm, 2.17 μm] for the manual measurements. The automated method resulted in narrower limits of agreement, indicating that it has a better repeatability than human raters.

The presented algorithm performs well in terms of measurement accuracy and reproducibility. The automated vessel measurement, with the validated performance, will be highly useful for many biological studies that require vessel diameter measurements over time.

BIOGRAPHICAL SKETCH

Jaesung Lee received a B.S. degree in Computer Engineering (summa cum laude) from the University of Michigan, Ann Arbor in 2004. In 2005, he started a M.S-Ph.D program in the School of Electrical and Computer Engineering at Cornell University. Inspired by the idea of computer-aided diagnosis, he became interested in the field of biomedical image analysis and joined the Vision and Image Analysis group headed by Dr. Anthony P. Reeves. As a first project in the group, he has worked on automated measurement of vessel diameter in close collaboration with Dr. Ingrid H. Sarelius at the University of Rochester Medical Center.

This thesis is dedicated to my family and friends.

ACKNOWLEDGEMENTS

First of all, I would like to acknowledge my advisor, Dr. Anthony P. Reeves, to whom I owe my deepest gratitude. This thesis would not have been possible without his encouragement, guidance, and support.

I would also like to give my gratitude to my other special committee members, Drs. Peter Doerschuk and Keith N. Snavely, for their time, support, and assistance, as well as to Drs. Ingrid H. Sarelius and William E. Crowe at the University of Rochester Medical Center for their assistance and feedback over the course of this work.

I thank my colleagues in Vision and Image Analysis group, Dr. Alberto Biancardi, Artit Jirapatnakul, Brad Keller, and Sergei Fotin, for their enlightening thoughts, friendship, and encouragement. I want to acknowledge other faculty members and students in the School of Electrical and Computer Engineering who provided me with helpful advice along the way.

Finally, I would like to thank my parents, my sister, and my other half for their endless support and trust.

TABLE OF CONTENTS

Biographical Sketch . . . iii
Dedication . . . iv
Acknowledgements . . . v
Table of Contents . . . vi
List of Tables . . . viii
List of Figures . . . ix

1 Introduction **1**
1.1 Background . . . 1
1.2 Previous Work . . . 2
1.3 Image Template Matching . . . 4
1.4 Image Registration . . . 6
1.5 Outline . . . 7

2 Methods and Materials **8**
2.1 Pre-processing . . . 8
2.2 Patch Definition . . . 9
2.2.1 Tracking . . . 11
2.2.2 Reference Patch . . . 13
2.2.3 Matching Metric . . . 14
2.3 Linked Tracking . . . 15

3 Parameter Optimization **18**
3.1 Reference frame and matching metric . . . 18
3.2 Patch size . . . 22

4 Experimental Design **25**
4.1 Evaluation of Accuracy . . . 25
4.1.1 Synthetic Image Sequences . . . 25
4.1.2 Intravital Image Sequences . . . 26
4.2 Evaluation of Repeatability . . . 26
4.3 Data Sets . . . 27

5 Results **31**
5.1 Accuracy . . . 31
5.1.1 Synthetic Image Sequences . . . 31
5.1.2 Intravital Image Sequences . . . 31
5.2 Repeatability . . . 33
5.3 Discussion . . . 37
5.3.1 Parameter Optimization . . . 37
5.3.2 Accuracy . . . 39
5.3.3 Repeatability . . . 40

6 Conclusion **41**
6.1 Contributions 41
6.2 Future Work 42

Bibliography **44**

LIST OF TABLES

3.1 Parameter sets for optimizing matching metric and α 19
3.2 Comparison of Trackings using different matching metrics 22

4.1 Criteria for qualitative evaluation 26

5.1 Qualitative evaluation on 20 cases 33

LIST OF FIGURES

1.1 Intravital microscopy: (a) mouse prepared for observation. [9] (b) view through the microscope. 2

2.1 Typical example of intravital image as seen through the microscope. The magnification on site is 1420x. 9
2.2 An overview of the proposed automated method. 9
2.3 Image registration. White box is drawn around a fixed region for better illustration. Running registration on an image sequence reduces the shift of the vessel, allowing for smaller search space and faster tracking. 10
2.4 User-specified parameters. The size of patches are determined by *xs* and *ys*, and the search area is determined by *h* and *v*. The parameter *in* is used to offset the patches. 10
2.5 Vessel diameter measurement by tracking two objects (patches). Simplified diagram of an image sequence with N frames is shown. 11
2.6 An overview of the tracking algorithm. Starting from the seed points on the first frame, the diameter is tracked on every subsequent frame in the video. 12
2.7 Effect of linked tracking. For each tracking method, frames 1 and 90 of the image sequence are shown. Tracking two patches separately can result in drifting of the patches (a). Linking the patches prevents the drifting (b). 16

3.1 Mean error for the cases with manual measurements: (a) 3 transmission cases and (b) 3 fluorescence cases. 10 parameter sets were created by varying the matching metric and α value. Refer to 3.1 for details of the parameter sets. The parameter sets that gave error greater than 10 μm were considered invalid tracking and were clipped in the plot. 20
3.2 Overall error for (a) all 6 cases, (b) transmission cases, (c) and fluorescence cases. The errors have been averaged for each parameter set. parameter sets. The parameter sets that gave error greater than 10 μm were considered invalid tracking and were clipped in the plot. 21
3.3 Mean measurement error vs. patch width 23
3.4 Maximum measurement error vs. patch width 23

4.1 First frames from 3 cases are shown. The images have been preprocessed so that the vessel runs horizontally. (a) Transmission microscopy image, (b) fluorescence microscopy image, and (c) synthetic image. Total of 10 cases for each category were considered for the evaluation of the automated method. For the fluorescence image, brightness has been adjusted for better visibility. 29

5.1 Tracking result for a synthetic image sequence, showing (a) diameter measurement plot through the entire sequence along with the screenshots at different frames:(b) Frame 1, (c) Frame 10, (d) Frame 25, and (e) Frame 30. Note that the automated measurements lie exactly on top of the ground truth. 32
5.2 Tracking result for a transmission microscopy image sequence, showing (a) diameter measurement plot through the entire sequence along with the screenshots at different frames: (b) Frame 1, (c) Frame 150, (d) Frame 250, and (e) Frame 350. 34
5.3 Tracking result for a fluorescence microscopy image sequence, showing (a) diameter measurement plot through the entire sequence along with the screenshots at different frames: (b) Frame 1, (c) Frame 150, (d) Frame 230, and (e) Frame 350. 35
5.4 Tracking result for the case that received the qualitative evaluation score of 3, showing (a) diameter measurement plot through the entire sequence along with the screenshots at different frames: (b) Frame 1, (c) Frame 95, (d) Frame 200, and (e) Frame 300. The correct tracking interfered as the lumen intensity brightens around frame 95. The erroneous measurement is marked with a circle in (a). 36
5.5 Inter-observer variability of manual measurements for a synthetic image sequence. 37
5.6 Bland-Altman analysis for two raters' measurements (a) and two automated measurements (b) using different parameters. Automated method has narrower range of diameter difference, indicating better reproducibility. 38

CHAPTER 1

INTRODUCTION

1.1 Background

In microcirculation studies, intravital video microscopy is widely used to observe mammalian vasculature *in vivo*. Typical procedure involves recording a video of microscopic observation and later analyzing the video. Among different uses of intravital imaging, many studies address how vessel diameter changes over time for the purpose of quantifying the effects of various causes.[11, 12, 13, 19, 21] The cremaster muscle, a thin layer of striated muscle that surrounds the testicle, is commonly used to observe the blood flow in a small mammals such as a mouse.[5, 7, 8, 9, 12, 13] Figure 1.1 shows a mouse prepared for observation and a view through the microscope.

Intravital image sequences typically span several minutes of time resulting in the acquisition of several thousand images. The current practice for measuring vessel diameter on a intravital video is for an operator to observe the entire video and manually place two lines on top and bottom vessel walls. The electronic calipers are used to adjust these lines in every image frame, and the entire procedure is a time-consuming task that is prone to measurement error and operator fatigue. This work proposes an automated method for measuring vessel diameter in intravital video microscopy.

There are several challenges in measuring vessel diameter with an accuracy. The frames often go out of focus, causing difficulties in finding the demarcation between the lumen and wall. Imaging noise resulting from the tissues above the

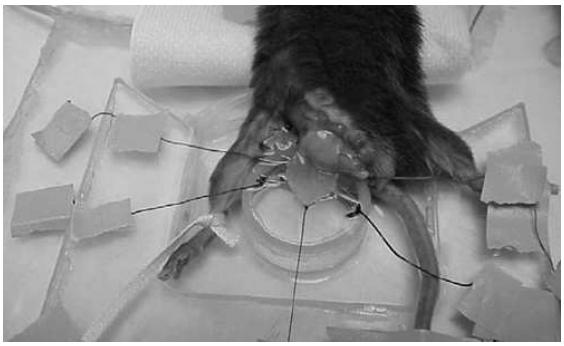

(a)

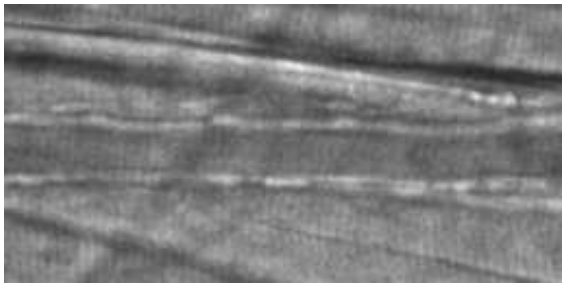

(b)

Figure 1.1: Intravital microscopy: (a) mouse prepared for observation. [9] (b) view through the microscope.

vessel and blood flowing through the vessel may also interfere with the accurate measurement of diameter. Finally, even a very little motion of the specimen during the observation causes significant shift in video microscopy due to high magnification.

1.2 Previous Work

While the specific task of measuring vessel diameter in intravital microscopy image sequences using computer vision techniques has not received much attention, there have been many proposed algorithms and techniques for object tracking and vessel measurements for other applications in other imaging

modalities which may be adapted to the problem domain of this paper.

Several previously proposed methods [22, 23, 24] attempted to locate the boundary of the vessel lumen and tissue using optimization algorithms.

Schmugge et al.[22] proposed a method for segmentation of vasculature in intravital microscopy. They first segmented the vessels with sharp edges using a snake-based algorithm.The vessels with less sharp edges were then located based on the ”bridges” between the segmented vessels. ROC analysis showed that their algorithm is able to get more vessels with lower sharpness.

Sonka et al.[23] developed an automated method for analysis of brachial ultrasound image sequences. Vessel tracking is achieved using a knowledge-based method. The method first identifies the vascular region of interest (ROI). This is followed by automated learning of vascular border properties which involves fine-tuning several matching parameters. The vessel borders are then detected in the image sequence using the globally optimal graph-search based border detection approach. Their automated method showed more accurate vessel diameter measurements in synthetic images than the two human observers. For the ultrasound image sequences, the method outperformed manual methods by displaying a decrease in analysis bias and increased reproducibility.

Tyml et al.[25] proposed a method to measure arteriolar diameter and hemodynamic resistance in intravital video microscopy images. Their algorithm required several markings of each edge along the lumen. The locations of vessel walls were estimated based on these markings, and the perpendicular distances between two walls were used to get a diameter estimate. Their method would require markings on every image frame of the sequence, thus making it unsuit-

able for automatic measurement in a sequence of multiple frames.

Accurate determination of vessel wall boundary can be used to estimate vessel diameter. However, the optimization algorithms work well only if there is a clear distinction between lumen and tissues surrounding the vessel.

Magers et al.[17] attempted to employ template matching algorithm to measure vessel diameter in microscopy images. Their algorithm used feature tracking with cross-correlation metric in one dimensional search space. Due to the constrained search space, the method would not be able to deal with the shifting of the vessel, which is common in intravital video microscopy. They validated the method with only 3 video microscopic images, while the manual repositioning of the wall locations were allowed.

1.3 Image Template Matching

The vessel diameter tracking can be thought of as tracking top and bottom vessel wall locations throughout the image sequence. Image template matching is a simple algorithm that is widely used to track the object of interest within the temporal sequence of images. The template matching algorithm finds the optimal match of the template according to a similarity measure.

The template matching algorithm has four main components: feature space, search space, search strategy, and similarity metric.[2] The feature space refers to the information present within the template, and the search space defines the area within which to search for the best match. The search strategy and the similarity metric determine how to search for the best match and how to determine

the similarity between the reference template and each match candidate.

There are various similarity measures to consider for template matching. Some widely used metrics include sum of absolute differences, sum of squared differences, and cross-correlation. For 2D discrete signals, such as image pixels, sum of squared differences (SSD) and correlation can be computed from Equations 1.1 and 1.2, respectively.

$$SSD(I_1, I_2) = \sum_{j=0}^{n-1} \sum_{i=0}^{m-1} (I_1(i, j) - I_2(i, j))^2, \tag{1.1}$$

$$corr(I_1, I_2) = \sum_{j=0}^{n-1} \sum_{i=0}^{m-1} I_1(i, j) I_2(i, j), \tag{1.2}$$

where I_1 and I_2 are two m x n subimages that are being compared.

Cross-correlation is known to be sensitive to noise and intensity variation, and normalized correlation is often used as a more robust measure. Normalized correlation can be computed from Equation 1.3.

$$norm\_corr(I_1, I_2) = \sum_{j=0}^{n-1} \sum_{i=0}^{m-1} \frac{I_1(i, j) I_2(i, j)}{\sigma_{I_1} \sigma_{I_2}}, \tag{1.3}$$

where σ_{I_1} and σ_{I_2} are the standard deviation of the pixel intensities within the subimages I_1 and I_2, respectively.

1.4 Image Registration

Image registration is a technique used when comparing the images taken at different times, by different sensors or from different viewpoints.[2] The registration algorithm tries to find the optimal transformation of an image with respect to the reference template. Image registration can be thought of as image template matching where the template of interest is the entire image.

One application of image registration is a stereo vision, where two cameras are used to get multiple views of one scene.[1, 15] The overlapping area in two images must be identified before the scene information can be retrieved from the images. Lucas et al.[15] proposed the image registration technique that can be applied to a stereo vision system. Their registration technique uses the spatial intensity gradient of the images to find the matches.

Image registration is widely employed in various modalities of medical images such as X-ray, computed tomography (CT), magnetic resonance (MR), and ultrasound.[3, 4, 14, 16] The need for image registration arises in clinical settings as proper integration of useful data obtained from the separate images is often desired.[18] Pluim et al.[20] proposed a rigid registration method for 3D clinical images including MR, CT, and positron emission tomography (PET). Their registration algorithm used both mutual information and gradient information present in the images.

For processing of a temporal image sequence, such as intravital video microscopy, each image frame needs to be registered to the first frame of the sequence. Ideally, the outcome of the registration on an intravital video microscopy would be a video with no vessel movement.

1.5 Outline

The previous methods using feature-based tracking cannot deal with shifting of the vessels which is common in the intravital video microscopy images. The work presented in this thesis focuses on the accurate measurement of the vessel diameter using image feature tracking technique that uses the appropriate features and can deal with the subject motion.

The goal of this work is to develop a computer algorithm which, once the diameter is marked in the first image frame, automatically computes the diameter for all subsequent image frames. The thesis is organized as follows: Chapter 2 contains the details of the algorithms, description of the data sets, and the design of the experiment. Chapter 5 discusses the results from the synthetic and intravital microscopy image sequences. Chapter 6 includes contributions of this work for the problem of vessel diameter measurement and future works.

CHAPTER 2

METHODS AND MATERIALS

Figure 2.1 shows a typical intravital image as seen through the microscope. The algorithm has been developed to fit the specific need of tracking vessel diameters in intravital image sequences. The automated method is composed of three steps: pre-processing, patch definition, and diameter tracking. The overview of the automated diameter measurement is outlined as a flowchart in Figure 2.2.

2.1 Pre-processing

A rectangular region of interest along the vessel is clipped from each image sequence and rotated so that blood flow along the vessel is orientated left-to-right and cropped to 512x256 pixels. The image frames are scaled from 10-bits to 8-bits and temporally filtered (5 frame median) resulting in a video with the frame rate of 6 frames per second.

The prepared image sequence is then registered to reduce horizontal shifts among image frames. Each image frame is shifted appropriately so that it yields the least difference when compared to the first frame of the sequence. The SSD matching metric was used to compare image frames to the first frame.

The effect of running image registration is illustrated in Figure 2.3. Black border is created as a result of shifting the image frame toward the best location. Registering the image sequence results in less horizontal movement of the vessel within the image sequence and therefore allows for smaller horizontal search space and faster tracking.

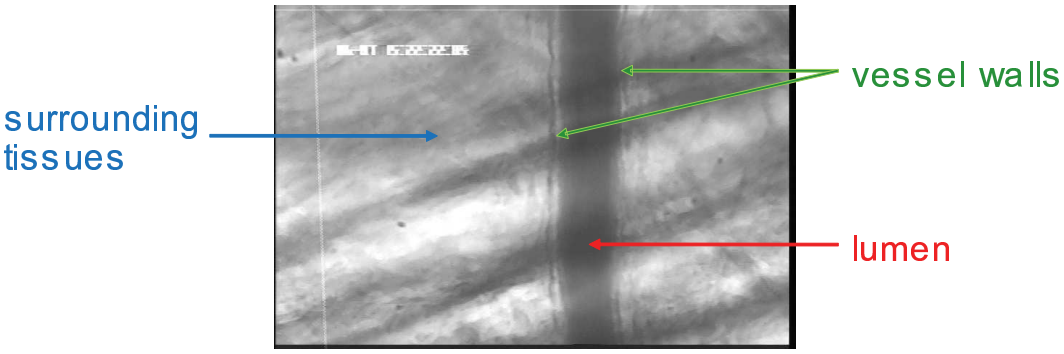

Figure 2.1: Typical example of intravital image as seen through the microscope. The magnification on site is 1420x.

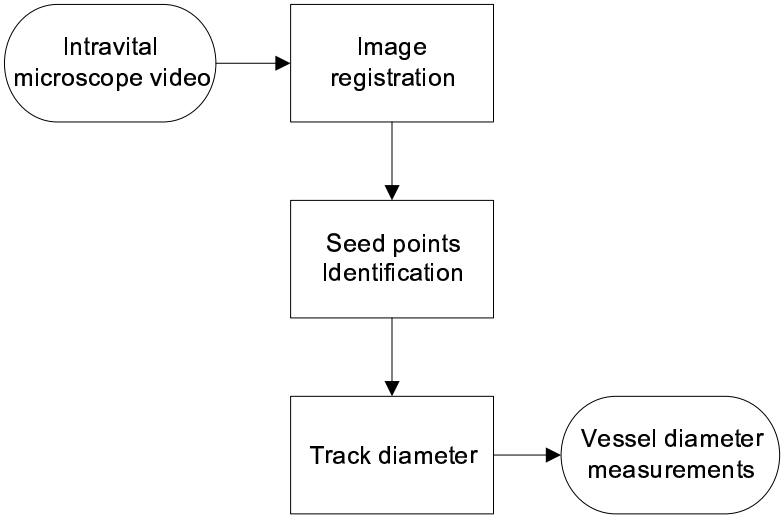

Figure 2.2: An overview of the proposed automated method.

2.2 Patch Definition

After the image registration process, the user must define two points in the first frame indicating the lumen diameter, one point on each side of the vessel lumen. For each point specified by the user, a surrounding box is established. Throughout this paper, these boxes are referred to as "patches". The properties of the patches are determined by the user-specified parameters (Figure 2.4). The

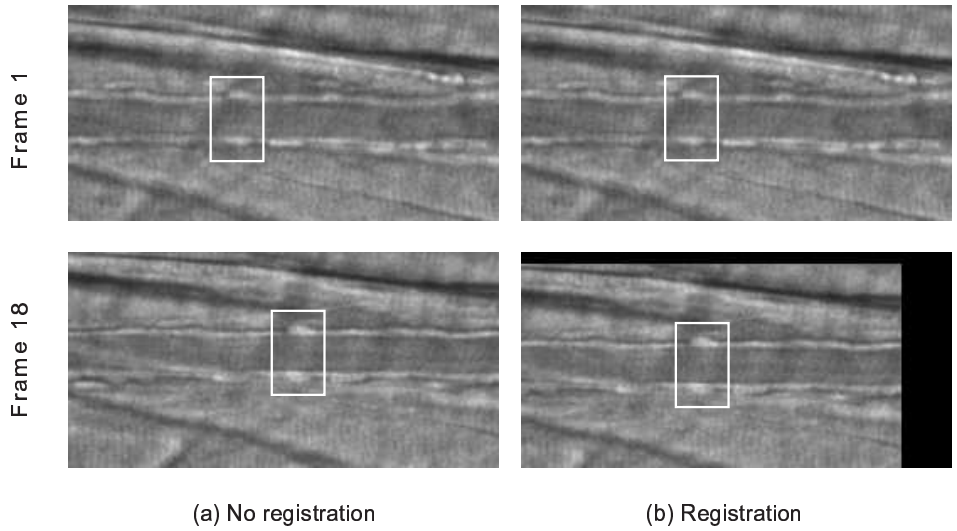

Figure 2.3: Image registration. White box is drawn around a fixed region for better illustration. Running registration on an image sequence reduces the shift of the vessel, allowing for smaller search space and faster tracking.

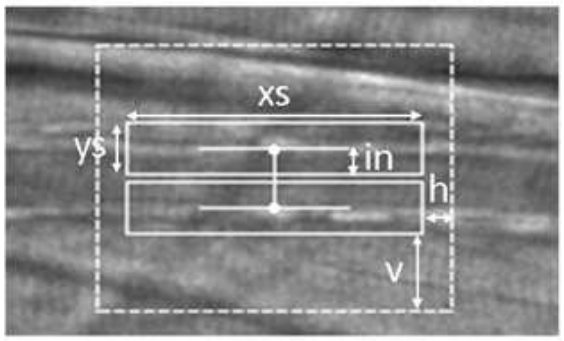

Figure 2.4: User-specified parameters. The size of patches are determined by *xs* and *ys*, and the search area is determined by *h* and *v*. The parameter *in* is used to offset the patches.

algorithm attempts to find the locations of the two patches in new frames based on the reference patches. The reference patch can be the corresponding patch in the first frame of the sequence, previous frame, or the blend of both. The details for defining reference patch is discussed in Section 2.2.1.

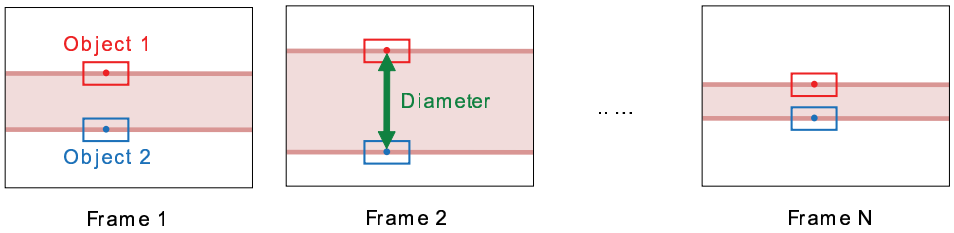

Figure 2.5: Vessel diameter measurement by tracking two objects (patches). Simplified diagram of an image sequence with N frames is shown.

The Euclidean distance between the two patches is considered the vessel diameter. It should also be noted that most of the interesting features lie outside of vessel walls. Blood may be flowing within the vessels, or the vessel may be so narrow that the patches include the opposite vessel wall. The patches may need to be shifted outward to reduce errors due to these distractions. The amount of shifting is user-specified with the parameter *in*, as shown in Figure 2.4.

The patch size and search space can be determined by observing each image sequence before running the tracking. The patch size needs to be thick enough to include the vessel wall and surrounding tissues and to be reasonably wide without overlapping any background patterns. The search space should be established so that the maximum movements of the patches were covered.

2.2.1 Tracking

After two patches have been established, the algorithm searches for new patch locations in the subsequent frames that best matches the reference patch. The template matching algorithm is used to track two patches throughout the entire video. The vessel diameter is estimated by taking the distance between top

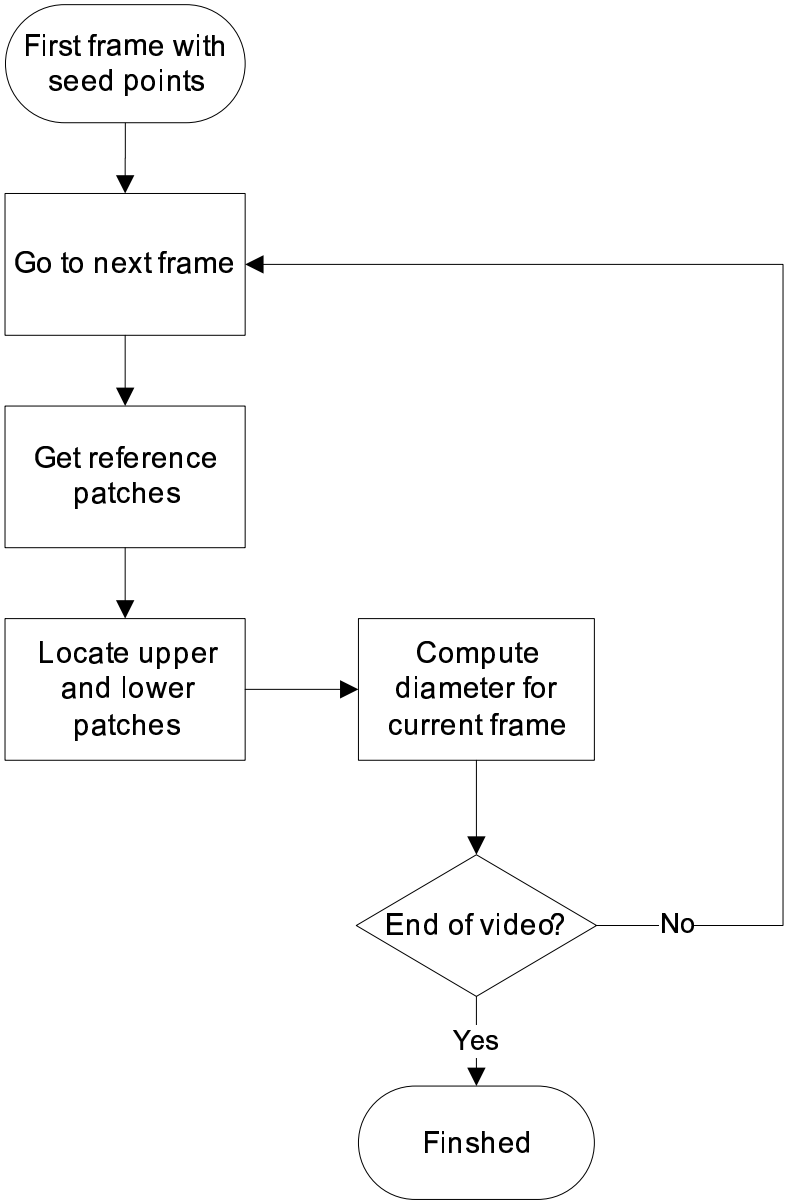

Figure 2.6: An overview of the tracking algorithm. Starting from the seed points on the first frame, the diameter is tracked on every subsequent frame in the video.

and bottom patches. The proposed approach is depicted in Figure 2.5, and the algorithm is outlined in Figure 2.6 as a flowchart.

To track the patches, it is necessary to define the reference patch and how to evaluate the closeness of the new patch candidate to the reference patch. In other words, the algorithm needs to know where to compare each candidate to (reference patch) and how to compare them (matching metric).

2.2.2 Reference Patch

Determining the best frame from which to get the reference patches is not an easy task and can vary for different cases. Always using the patches in the first frame may work well for the cases where the shapes of vessel walls do not vary across the image sequence. Using the patches in the previous frame has an advantage that it can adapt to varying intensities throughout the sequence. It may also be useful to define the reference patches to be a blend of these two options.

To parameterize how the reference patches are defined, a variable α is introduced. Equation 2.1 show how α is used to define the reference patch at frame t. The parameter α controls how much patch information is coming from the located patches from the previous frame and how much is coming from the reference patches used for the previous frame.

$$RP(t) = \alpha \cdot P(t-1) + (1-\alpha) \cdot RP(t-1), t > 1, \tag{2.1}$$

where $RP(t)$ is the reference patch used in frame t, and $P(t)$ is the best matching

patch in frame t using $RP(t)$ as a reference. $P(1)$ and $RP(1)$ correspond to user-defined seed points in the first frame of the sequence. Both RP and P represent the set of pixel intensities for given patches, and the operations in Equation 2.1 are done for each pixel in the patches. The reference patch will always be the first frame's patch when α is zero and the previous frame's patch when α is one.

2.2.3 Matching Metric

Two matching metrics considered in the experiments are based on the SSD (sum of squared differences) and normalized correlation. Equations 2.2 and 2.3 show how these metrics are computed. Both metrics are normalized to range from 0 to 1. The user can specify which metric is used for locating the best matching patches in the image frames.

$$Metric_{SSD}(X, Y) = 1 - \frac{1}{MAX} \sum_{j=0}^{n-1} \sum_{i=0}^{m-1} (X(i, j) - Y(i, j))^2, \tag{2.2}$$

$$Metric_{corr}(X, Y) = 0.5 + \sum_{j=0}^{n-1} \sum_{i=0}^{m-1} \frac{X(i, j)Y(i, j)}{2\sigma_X \sigma_Y}, \tag{2.3}$$

where X represents the current patch of interest being compared to the reference patch Y. In both equations, X and Y represent set of pixel intensities for given patches, and the operations are done for each pixel in the patches. In Equation 2.2, MAX is the maximum possible SSD between X and Y and is used as a normalizing constant (for an 8-bit image, 255 x patch area). The implicit assumptions are that the gray level pattern is approximately constant between

Algorithm 1: Linear exhaustive search with linked patches

$Match_{max} = -1$

$p1 = p(x, y_1)$

$p2 = p(x, y_2)$

for all $x_i \in$ *search area* **do**

$y_{1j} = argmax_y\{Match(p1, p(x_i, y)) \mid y \in \text{search area}\}$

$y_{2j} = argmax_y\{Match(p2, p(x_i, y)) \mid y \in \text{search area}\}$

$Match_i = Match(p1, p(x_i, y_{1j})) + Match(p2, p(x_i, y_{2j}))$

if $Match_i > Match_{max}$ **then**

$Match_{max} = Match_i$

$x' = x_i; \quad y'_1 = y_{1j}; \quad y'_2 = y_{2j};$

end if

end for

$p1' = p(x', y'_1)$

$p2' = p(x', y'_2)$

successive frames and that local texture contains sufficient unambiguous information [10].

2.3 Linked Tracking

If separate feature tracking is used for each patch, it is possible that two patches will drift toward opposite directions as image frame progresses (Figure 2.7a). This is especially true for image sequences with shifting vessels. This will cause inaccurate estimation of vessel diameter, as the correct diameter is the length

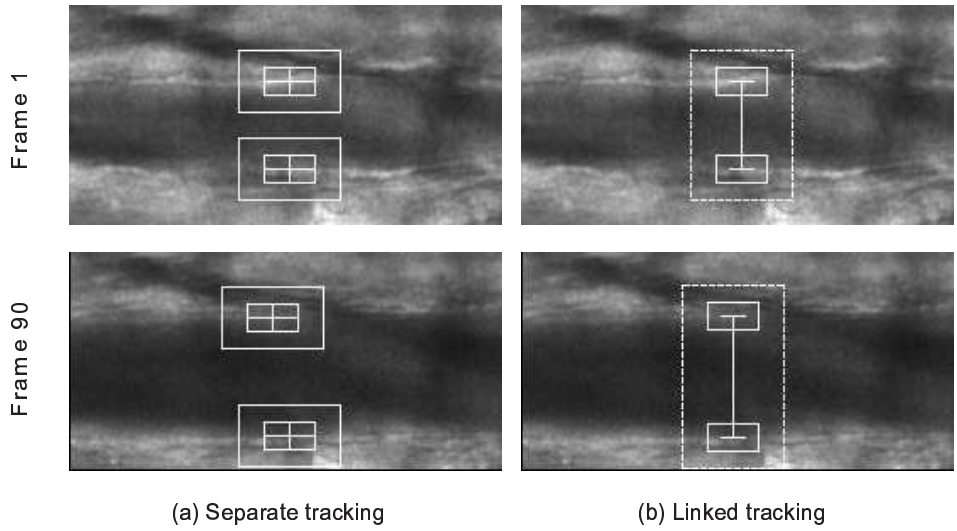

Figure 2.7: Effect of linked tracking. For each tracking method, frames 1 and 90 of the image sequence are shown. Tracking two patches separately can result in drifting of the patches (a). Linking the patches prevents the drifting (b).

of a line perpendicular to vessel walls. To address this problem, the horizontal motion of the two patches is linked. Because the patches are linked, a new matching metric has to be introduced. The algorithm uses the sum of the matching metrics for two patches being considered.

Instead of finding the best x and y coordinates separately for each patch, the best x coordinate is sought to maximize the matching metric for both patches, while for each patch the best y coordinate is sought separately within each x coordinate in search space. In other words, given two patches $p1(x, y_1)$ and $p2(x, y_2)$, the best matching locations $p1'(x', y_1')$ and $p2'(x', y_2')$ in the following frame are found using linear exhaustive search. The procedure for carrying out linear exhaustive search is outlined in Algorithm 1. Linking the patches in this way prevents them from drifting toward opposite directions. If the region of interest has shifted horizontally in the following image frame, both patches will

shift horizontally by the same amount. Figure 2.7 shows the effect of linking the patches.

CHAPTER 3

PARAMETER OPTIMIZATION

Three parameters have been optimized for tracking vessel diameter: reference frame, matching metric, and patch size. To optimize tracking parameters, 6 intravital image sequences, 3 transmission and 3 fluorescence, were manually measured by an experienced rater.

The interactive web-based marking interface was developed for this purpose. The rater's task was to identify the same two points in all frames for each intravital sequence. For each case, a line was drawn in every 10 frames to indicate the diameter of the vessel. For these cases, mean errors for the diameter measurements were computed with respect to the manual ground truth, while varying the parameters to find the optimal value.

3.1 Reference frame and matching metric

First, the optimal values for reference frame (α) and the better matching metric to use for tracking were determined.

The patch size was fixed to 125x20 pixels, and the trackings were run with five different α values in increments of 0.25 using both SSD and correlation metrics. This gave the trackings with 10 different parameter settings. The SSD matching metric was used for the parameter sets 0-4, and correlation metric was used for the parameter sets 5-9. The $\alpha = 0$ was used for the sets 0 and 5. The value of α was incremented by 0.25 for the sets 1-4 and 6-9. Table 3.1 summarizes 10 different parameter sets.

Table 3.1: Parameter sets for optimizing matching metric and α

Parameter set	Matching metric	α
0	SSD	0
1		0.25
2		0.5
3		0.75
4		1
5	Correlation	0
6		0.25
7		0.5
8		0.75
9		1

Figure 3.1 shows mean errors for 6 cases tracked using 10 parameter sets. To compare the overall performance for the parameter sets, average mean error for all 6 cases was computed for each parameter set (Figure 3.2a). Further, the performance on two types of images, transmission and fluorescence, were also plotted against 10 parameter sets (Figures 3.2b,c). When all 6 cases were considered, using the correlation metric with $\alpha = 0.0$ tracked the diameter with the smallest error. However, when only transmission microscopy cases are considered, tracking using the SSD metric with $\alpha = 0.0$ gave the best performance. For fluorescence microscopy cases, tracking using the correlation metric with $\alpha = 0.0$ resulted in the best performance.

The trackings with the best performance were always run with α value of 0.0. This indicates that the diameter measurement yields the least error when

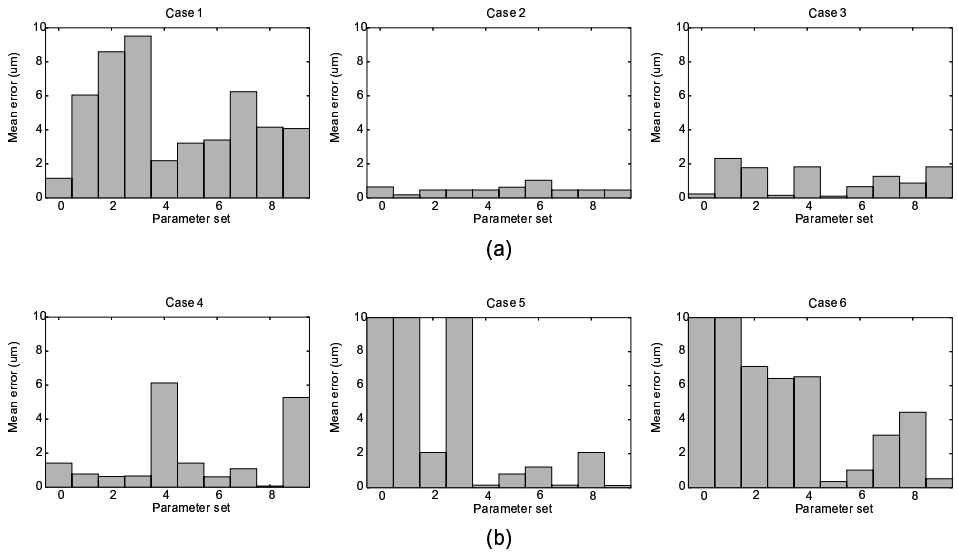

Figure 3.1: Mean error for the cases with manual measurements: (a) 3 transmission cases and (b) 3 fluorescence cases. 10 parameter sets were created by varying the matching metric and α value. Refer to 3.1 for details of the parameter sets. The parameter sets that gave error greater than 10 μm were considered invalid tracking and were clipped in the plot.

the reference patch is taken from the previous frame. For each matching metrics (with $\alpha = 0.0$), the mean measurement error is reported in Table 3.2 for transmission, fluorescence, and all image types. From Table 3.2, it is evident that using the SSD-based metric is optimal for tracking the vessel diameter in transmission microscopy, while the correlation based metric is optimal for tracking in fluorescence microscopy.

The reason why the correlation metric works better than the SSD metric in fluorescence microscopy seems to be the nature of fluorescence images. In fluorescence images, the vessel walls appear as bright region on dark background, and the majority of the background pixels have intensities close to zero. The correlation metric indicates the similarity in the image pattern, rather than the

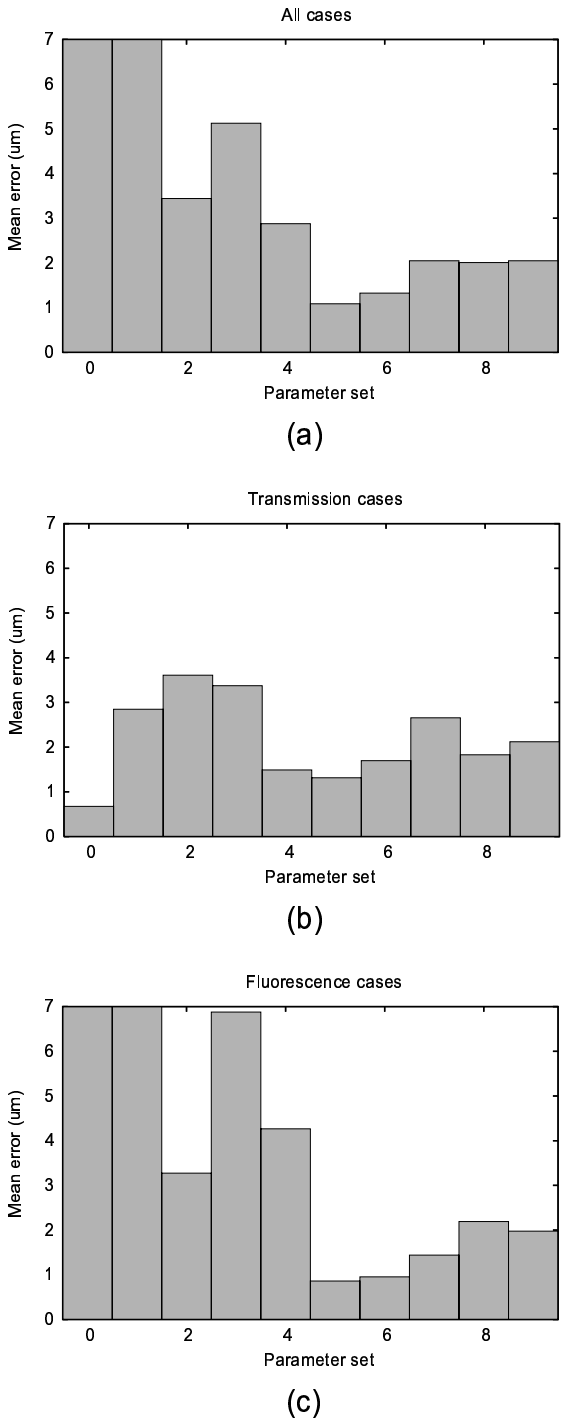

Figure 3.2: Overall error for (a) all 6 cases, (b) transmission cases, (c) and fluorescence cases. The errors have been averaged for each parameter set. parameter sets. The parameter sets that gave error greater than 10 μm were considered invalid tracking and were clipped in the plot.

Table 3.2: Comparison of Trackings using different matching metrics

Image type	Mean error with SSD metric (μm)	Mean error with correlation metric (μm)
All	3.44	1.70
Transmission	0.67	1.31
Fluorescence	3.27	0.86

similarity of individual pixel intensities. However, in transmission images, a wider range of intensity values are present, and counting the differences in individual pixel intensities seem to result in better matches.

3.2 Patch size

The patch height should be tall enough to cover the entire vessel wall area and was fixed to 20 pixels. The optimal value of patch width was found by comparing the measurement results from the trackings with different patch widths. The α was set to zero, and the correlation metric was set to the optimal one for each image type as found in the previous section.

The patch width was varied from 25 pixels to 250 pixels in increments of 25 pixels. For each case, mean error was calculated based on the ground truth measurements. The average error for measurements in 6 cases was plotted against the patch width (Figure 3.3). Since robustness is important for measuring vessel diameter, the maximum error in six cases was also plotted against the patch width (Figure 3.4).

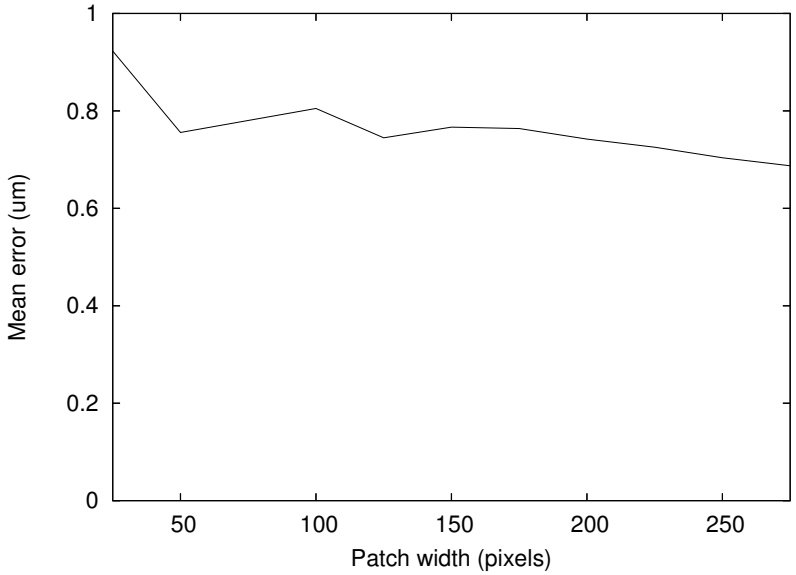

Figure 3.3: Mean measurement error vs. patch width

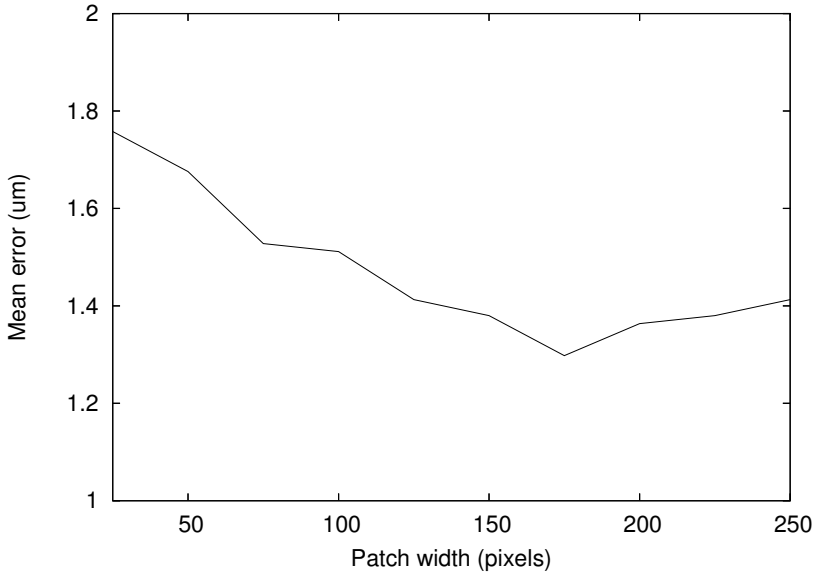

Figure 3.4: Maximum measurement error vs. patch width

The range of the average errors was under 0.1 μm for the patch width greater than 100 pixels. Small patch width, such as 25 pixels, resulted in the worst average performance, as expected since not enough features are included in the patch. The maximum error among the six cases is also worth considering for assessment of the algorithm's robustness. It is suspected that the tracking is not as robust when ran with the large patch width because it may include the background pattern that does not belong to the vessel wall itself.

The smallest maximum error was observed for the tracking with the patch width of 175. Although the smallest mean error was not observed with this patch width, it deviated by less than 0.1 μm from the best one. Therefore, 175x20 pixels was determined to be the optimal patch size and was used for the experiments.

CHAPTER 4

EXPERIMENTAL DESIGN

The experiments were designed to determine whether the automated diameter tracking algorithm correctly measures the vessel diameter through each intravital microscopy image sequence. Better tracking of the vessel should result in more accurate and consistent determination of the vessel diameter. Specifically, accuracy and repeatability of the automated method were assessed.

4.1 Evaluation of Accuracy

First set of experiments were to determine the accuracy of the automated measurements. The automated method was evaluated with 10 synthetic image sequences and 20 intravital image sequences.

For each image sequence, two seed points were determined by the author so that the points lie on the borders between the lumen and the vessel walls. The optimized parameters, as determined in the previous section, were used to run trackings. The SSD matching metric was used for tracking transmission microscopy images, and the correlation matching metric was used for fluorescence images. For all images, the patch size used for the experiments was 175x20 pixels, and the α value was set to 0.0.

4.1.1 Synthetic Image Sequences

The automated method was first tested with the synthetic sequences to evaluate the accuracy of the measurements. The ground truth measures were known

for the synthetic data, and mean error was calculated for each sequence. Establishing ground truth for the intravital image sequences is a difficult task due to large number of image frames per case.

4.1.2 Intravital Image Sequences

To evaluate the performance on the intravital cases, the rater qualitatively evaluated the tracking results for 20 cases. The rater visually inspected the tracking results and rated each case on a scale of 1-5. The description of the scale is outlined in Table 4.1. The scores 4-5 were given to usable diameter measurements, the scores 1-2 were given to unusable results, and the score of 3 indicated the midpoint between usable and unusable results.

Table 4.1: Criteria for qualitative evaluation

Score	Description
5	Tracking is good for the entire sequence
4	There are frames where the measurement is off by 3 or less pixels
3	There are frames where the measurement is off by more than 3 pixels
2	There are several frames where the measurement is completely off
1	Loses track completely and shows random behavior

4.2 Evaluation of Repeatability

This part of the experiment compared the repeatability of the manual and automated measurement of vessel diameter. Total of 7 intravital image sequences

were considered for the experiments. Two raters independently marked the vessel diameters throughout each image sequence, as described in Chapter 3. Further, the automated method was run twice on each image sequence with different seed point locations.

Bland-Altman analysis was used to evaluate the inter-observer variability of manual and automated diameter measurements on intravital image sequences. Bland-Altman analysis plots the difference for each pair of measurements against the average of the pair and gives the lower and upper limits of agreement between two sets of measurements (e.g. rater1 vs. rater2 or automated1 vs. automated2). The plots were generated for both measurement methods, and the limits of agreement were compared.

4.3 Data Sets

All images were acquired on an Olympus BX50WI microscope through an Olympus UMPlanF1 water immersion objective (20x, 0.5 NA). Images were directed to a Nipkow disk scanning confocal head (CSU 22, Yokogawa) connected to an intensified CCD camera (XR Mega10, Stanford Photonics). The 10-bit images were digitally streamed to a terabyte RAID disk as 16-bit TIFF files at 30 frames per second (Piper software, Stanford Photonics).

There were two categories of intravital microscopy images, transmission and fluorescence. Fluorescence confocal images were collected from endothelial cells loaded with the calcium-sensitive fluorophore, fluo-4 [6] that were excited with the 488 nm laser line from Argon laser (DLS300Ar, Dynamic Laser). Non-confocal transmission images were acquired through the confocal optical path

using brightfield illumination. Diameter changes were invoked with a pressure pulse of acetylcholine (20 pounds/in^2, 0.5 seconds).

A rectangular region of interest along the vessel is clipped from each image sequence and rotated so that blood flow along the vessel is orientated left-to-right and cropped to 512x256 pixels. The images are scaled from 10-bits to 8-bits and temporally filtered (5 frame median) resulting in a video with the frame rate of 6 frames per second.

Confocal and transmission images were processed and converted to 8-bit TIFF stacks using ImageJ software macros. A rectangular region of interest along the vessel was clipped from each image sequence and rotated so that blood flow along the vessel was orientated left-to-right, cropped to 512x256 pixels, and scaled from 10-bits to 8-bits and temporally filtered. The final images had 410 frames with the resolution of 0.69 μm/pixel. The images were then uploaded to the server using a web-based interface.

Both types of microscopy images were used for automated measurements of vessel diameter. The complete intravital microscopy data set was composed of 10 transmission microscopy images and 10 fluorescence microscopy images. Figure 4.1 shows the example of transmission and fluorescence images that have been pre-processed.

For determination of accuracy, 10 synthetic image sequences were created. Each synthetic image sequence had 30 frames with resolution of 256x128 pixels. The synthetic sequences were created by taking a portion of the background from a real image sequence and overlaying two higher intensity lines meant to represent the vessel walls. The width of the walls was varied randomly by

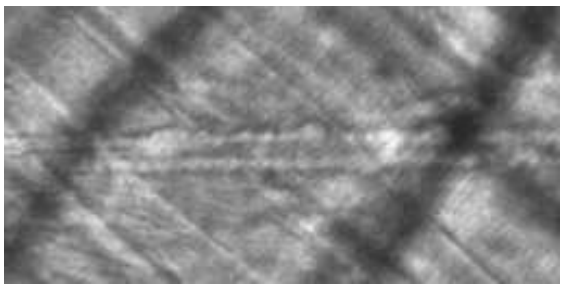

(a) Transmission

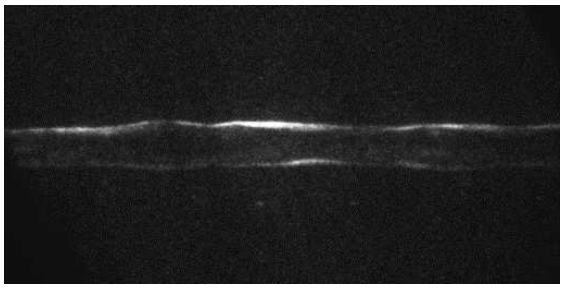

(b) Fluorescence

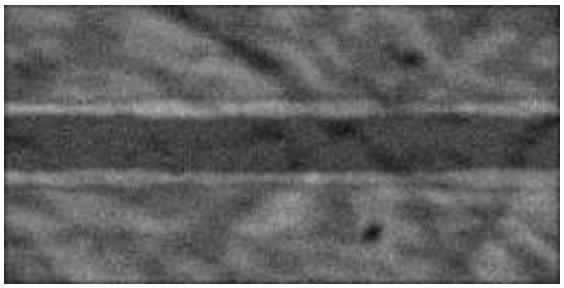

(c) Synthetic

Figure 4.1: First frames from 3 cases are shown. The images have been preprocessed so that the vessel runs horizontally. (a) Transmission microscopy image, (b) fluorescence microscopy image, and (c) synthetic image. Total of 10 cases for each category were considered for the evaluation of the automated method. For the fluorescence image, brightness has been adjusted for better visibility.

one pixel in either direction along the length of the vessel. The diameter of the vessel was also randomly varied throughout the sequence by up to five pixels per frame, and the entire vessel was shifted randomly in horizontal direction. Gaussian noise was then applied to the images with a variance in the range of 5.0 to 10.0 in 1.25 increments. To better model the intensity profile of the real vessel walls, Gaussian blurring with a σ of 1.0 was applied to the final images. A frame from one of the generated synthetic image sequences is depicted in Figure 4.1c.

CHAPTER 5

RESULTS

5.1 Accuracy

The accuracy of the method has been evaluated using both synthetic and intravital image sequences. The average mean error was calculated for the synthetic cases, and the qualitative evaluation was performed for the intravital cases.

5.1.1 Synthetic Image Sequences

All synthetic image sequences were tracked successfully with the automated method. For synthetic cases, the results were very similar when using different parameter settings, and the reported numbers are the results of running the algorithm using 175x20 pixels patches, the SSD matching metric, and α value of 0.0. The average mean error in 10 cases was 0.0 pixel, indicating that the algorithm was able to track diameter perfectly for all the frames in all cases. The resulting plot of the automated diameter measurements in a synthetic image sequence is shown in Figure 5.1.

5.1.2 Intravital Image Sequences

The resulting plot of the automated diameter measurements along with the screenshots of different frames is shown in Figure 5.2 (transmission image) and Figure 5.3 (fluorescence image).

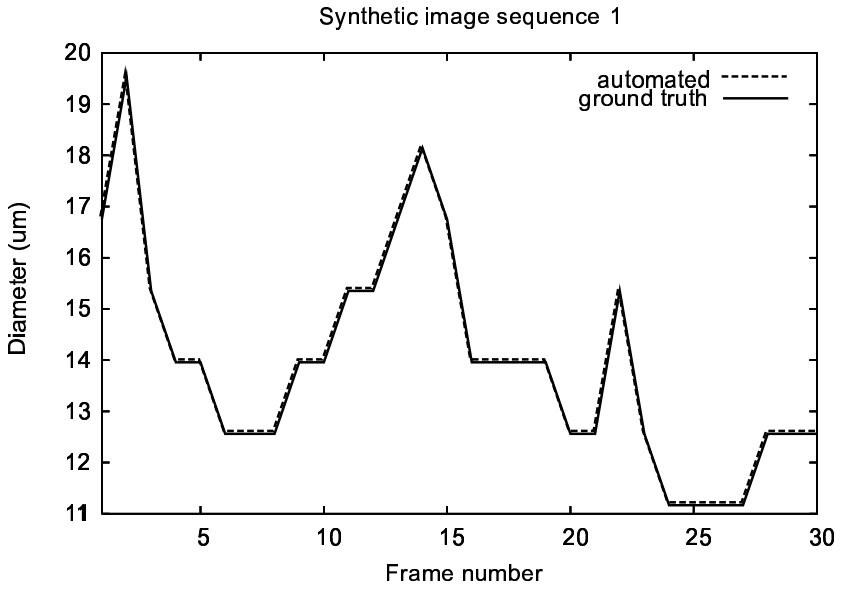

(a)

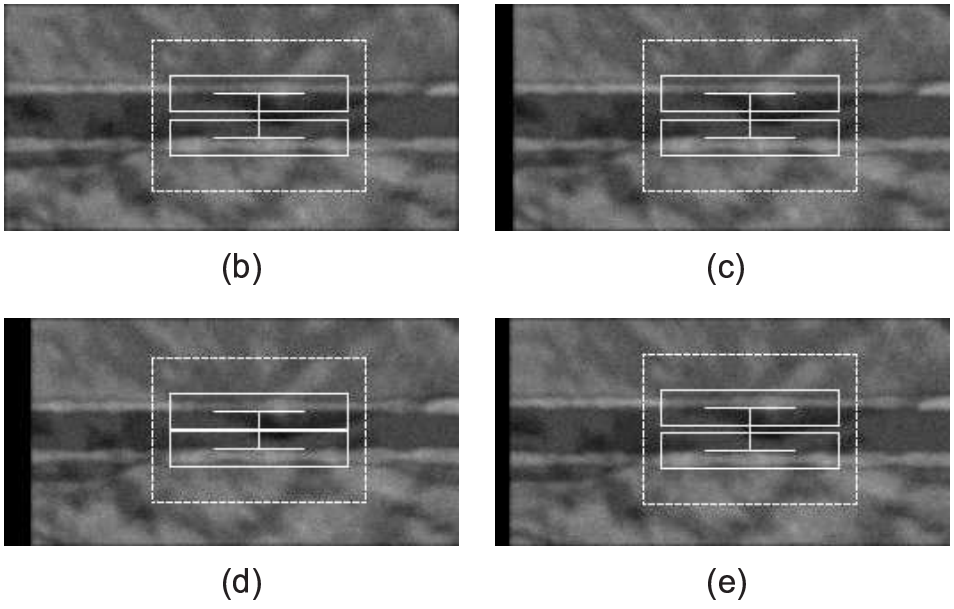

(b) (c)

(d) (e)

Figure 5.1: Tracking result for a synthetic image sequence, showing (a) diameter measurement plot through the entire sequence along with the screenshots at different frames:(b) Frame 1, (c) Frame 10, (d) Frame 25, and (e) Frame 30. Note that the automated measurements lie exactly on top of the ground truth.

The result of qualitative evaluation on 20 intravital cases is shown in Table 5.1. Trackings on 19 intravital images were evaluated with scores 4 or above, and there was one case with the score of 3. The case that received the score of 3 is shown in Figure 5.4.

Table 5.1: Qualitative evaluation on 20 cases

Transmission cases	T1	T2	T3	T4	T5	T6	T7	T8	T9	T10	Avg
Score	4	3	4	4	4	5	5	5	5	4	4.3
Fluorescence cases	F1	F2	F3	F4	F5	F6	F7	F8	F9	F10	Avg
Score	5	5	4	5	5	5	5	5	5	5	4.9

5.2 Repeatability

The manual measurements by two raters were plotted for a synthetic sequence to illustrate the variability of the manual measurements by two raters (Figure 5.5).

Bland-Altman analysis was used to quantify and compare the repeatability of manual and automated methods. Both manual and automated methods had two measurements as described in Section 4.2. Using two measurements, the diameter differences were plotted against the average of two for both methods (Figure 5.6). 95% of the measurement differences for the automated method lied between -1.36 and 1.52 μm, compared to -3.08 and 2.17 μm for the manual method by the raters.

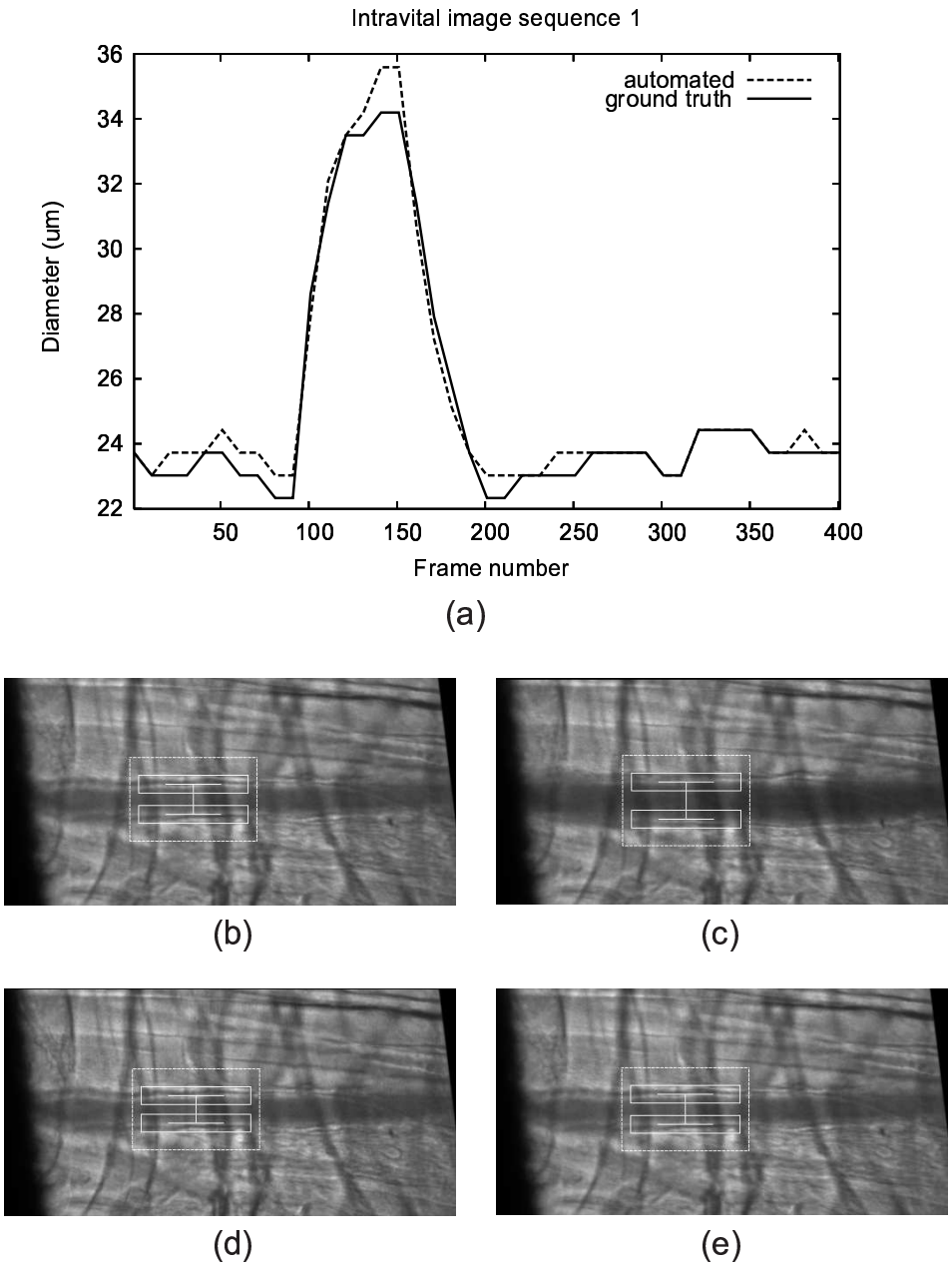

Figure 5.2: Tracking result for a transmission microscopy image sequence, showing (a) diameter measurement plot through the entire sequence along with the screenshots at different frames: (b) Frame 1, (c) Frame 150, (d) Frame 250, and (e) Frame 350.

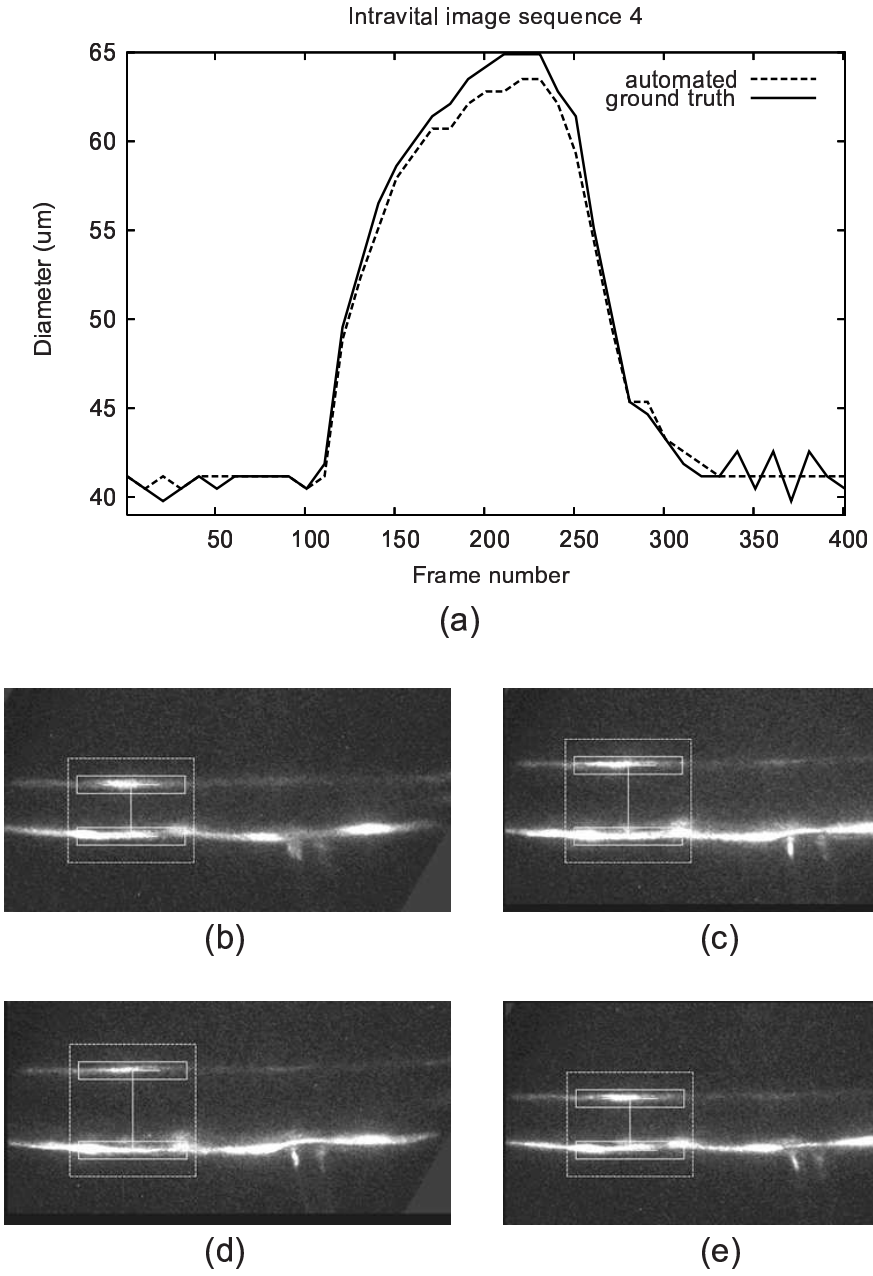

Figure 5.3: Tracking result for a fluorescence microscopy image sequence, showing (a) diameter measurement plot through the entire sequence along with the screenshots at different frames: (b) Frame 1, (c) Frame 150, (d) Frame 230, and (e) Frame 350.

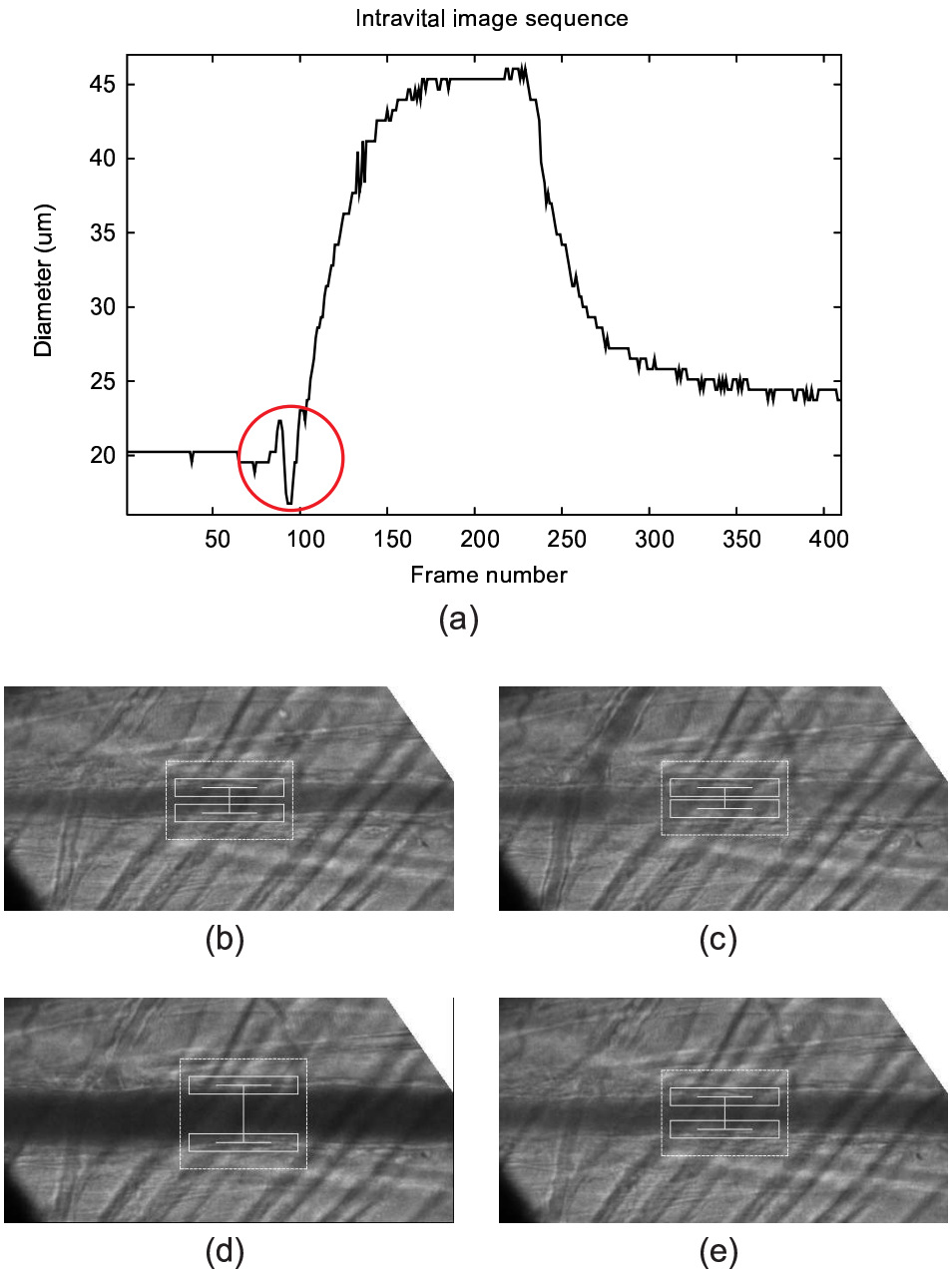

Figure 5.4: Tracking result for the case that received the qualitative evaluation score of 3, showing (a) diameter measurement plot through the entire sequence along with the screenshots at different frames: (b) Frame 1, (c) Frame 95, (d) Frame 200, and (e) Frame 300. The correct tracking interfered as the lumen intensity brightens around frame 95. The erroneous measurement is marked with a circle in (a).

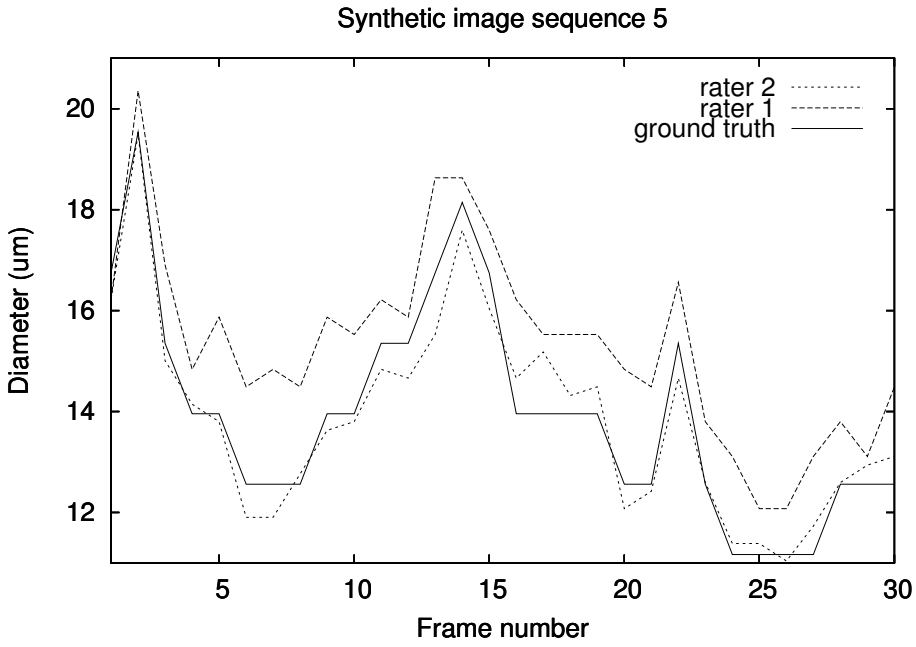

Figure 5.5: Inter-observer variability of manual measurements for a synthetic image sequence.

5.3 Discussion

5.3.1 Parameter Optimization

For two types of intravital image sequences, diameter tracking with different parameter sets gave the optimal results (Figure 3.2). For transmission microscopy, using the SSD matching metric resulted in the lowest error, while the correlation matching metric gave the lowest error for fluorescence microscopy.

It was shown that using the SSD metric (parameter sets 0-4) for tracking on fluorescence images yielded poor performance when compared to the tracking with correlation metric (parameter sets 5-9). It is speculated that the correlation metric works better than the SSD metric in fluorescence microscopy because the

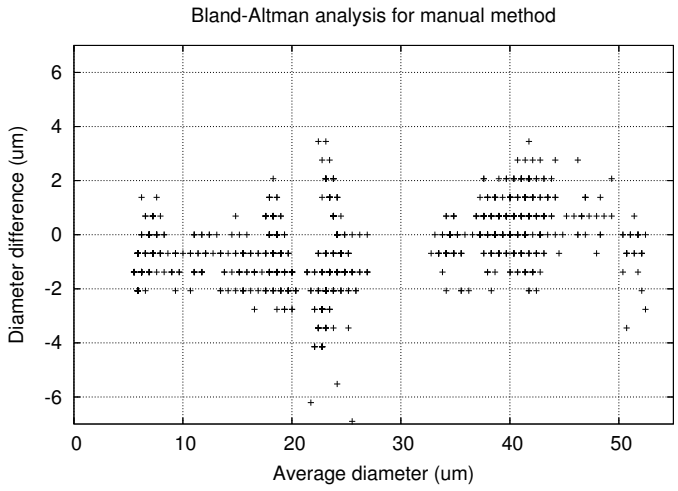

(a) Manual

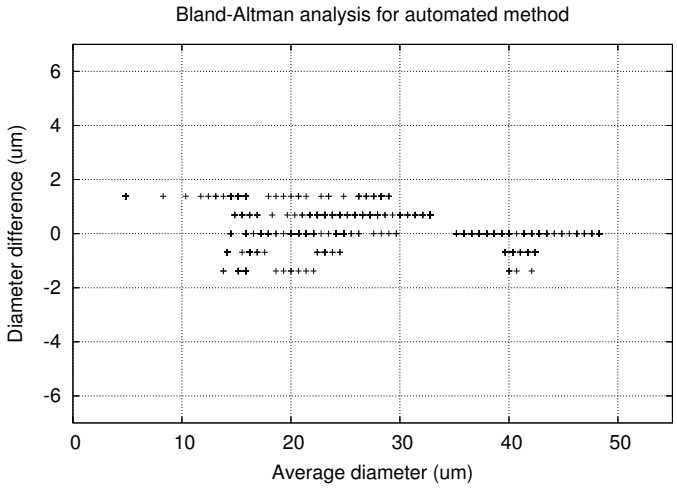

(b) Automated

Figure 5.6: Bland-Altman analysis for two raters' measurements (a) and two automated measurements (b) using different parameters. Automated method has narrower range of diameter difference, indicating better reproducibility.

majority of the pixels in fluorescence microscopy have intensities close to zero.

Tracking using α values greater than 0.0 did not lower the mean error for either image type. For both image types, setting α to 0.0 gave the best results. This indicates that using the previous frame's patch as a reference yields the

best performance. The reason why any degree of frame averaging for the reference patch does not help seems to be the high on-site magnification of the microscopic image data. Even tiny movement of the subject can affect how a image frame appears and result in some distortion of particular frame.

The patch size was also varied, but on average no significant advantage was observed when using smaller or larger patches. However, it was observed that the mean error increases when the patch size becomes too small. The suspected reason for this is that small patches may not capture enough features of the vessel wall. Also, maximum error increased when the patch size was too large. The inclusion of the unnecessary background patterns with the large patch size seems to be the cause of this increase in maximum error.

5.3.2 Accuracy

The automated method was able to successfully track vessel diameter on all synthetic image sequences in the presence of random translational movement and varying amounts of noise. The mean error of 0.0 pixel was achieved with the automated method for 10 synthetic cases, indicating the high accuracy of the measurements.

For the qualitative analysis on 20 intravital cases, the diameter trackings on 19 cases were evaluated as "usable" (score of 4 or higher) by an experienced rater, and the average score was 4.6.

However, the tracking result for one case received a score of 3 (Figure 5.4), indicating that there were frames where the measurements were off by 3 or more

pixels. For this particular case, there was a noticeable intensity change in bottom half of the lumen in frames 90-100. The algorithm was unable to correctly track the bottom vessel wall due to the hazy appearance of the lumen in these frames. Although the measurements were off for these frames, it recovered once the lumen intensity recovered to the original appearance at frame 100.

5.3.3 Repeatability

The repeatability of the automated diameter measurements was compared with that of the manual measurements. From Figure 5.5, the variability between two human raters can be observed. Although two raters performed the manual diameter measurement starting at the same initial diameter, the measurements start diverging after first two image frames. At 6th frame of the image sequence, two measurements differ by more than 2.0 μm.

The Bland-Altman plots (Figure 5.6) show the differences in two measurements for both manual and automated methods. The automated method has the narrower 95% limits of agreement, indicating that it is more robust than the manual method.

CHAPTER 6

CONCLUSION

An accurate and robust measurement of vessel diameter is very important in obtaining quality results in microcirculation studies. Very little previous work has been done on this task, though there has been much work on measuring diameters in other imaging modalities for applications such as measuring arteries in ultrasound images, retinal vessels, and airways in CT. In this work, an algorithm was developed and validated for accurate measurement of the vessel diameter from the intravital microscopy.

6.1 Contributions

The automated vessel measurements in intravital images will be highly useful for many biological studies that require vessel diameter measurements over time. The developed algorithm employs the variation of the template matching algorithm to solve the problem of measuring vessel diameter in image sequences. The algorithm starts with the user-defined seed points on top and bottom wall boundaries. The template matching algorithm attempts to track two windows that are established around the seed points throughout the image sequence. Then the vessel diameter is estimated by taking the distance between the two points.

The effect of different parameters for the template matching algorithm on the performance of vessel diameter measurement has been explored, and the optimal parameters for different types of microscopy were found. Specifically, the effect of matching metric and the patch size was assessed as well as the effect

of temporal averaging for the reference template.

The method has been validated using 20 intravital microscopic videos and 10 synthetic videos. The results show that the automated measurement is in agreement with the manual measurement, which is the current standard. From the experiments using both fluorescence confocal and non-confocal transmission microscopy images, the results show that automated method can measure the diameter with a mean error of 0.68 μm on the fluorescence images and 0.86 μm on the transmission images.

It was also shown that the automated method has higher repeatability for the diameter measurement. The automated and manual measurements were taken twice each on the intravital microscopic videos, and the limits of agreement on the difference of the two measurements were [-1.36 μm,1.52 μm] for the automated method and [-3.08 μm, 2.17 μm] for the manual method.

6.2 Future Work

Possible areas for future work include automatic determination of patch size and search area, reduction of intensity variation among frames, and applying the technique for measuring a quantity in other image modalities.

In this work, an optimized patch size and fixed search area were used for all intravital videos. The patch size was optimized using a set of intravital videos, and the search space was chosen to cover the maximum movement. The task of choosing the optimal parameter values for individual cases may be automated as a future development.

In order to improve the performance, the variation of intensities in different image frames may be addressed. The intensity of each image frame needs to be calibrated to have same overall brightness as the reference image frame, possibly the first image. Mean pixel intensity may be considered in each image frame to reduce the variation. With less intensity variation among frames, the tracking algorithm will perform more robustly.

The tracking technique with the linked windows may be useful for applications using image modalities other than intravital microscopy. An example would be the tracking of the valve openings in cardiac ultrasound video. For this work, the constraint was placed on the horizontal movement of each window with respect to one another. Depending on the application, the constraints added to the conventional template matching algorithm may be varied.

BIBLIOGRAPHY

[1] N. Ayache and B. Faverjon. Efficient registration of stereo images by matching graph descriptions of edge segments. *International Journal of Computer Vision*, 1(2):107–131, 1987.

[2] L.G. Brown. A survey of image registration techniques. *ACM Computing Surveys*, 24(4):325–376, 1992.

[3] R.W. Cox and A. Jesmanowicz. Real-Time 3D Image Registration for Functional MRI. *Magnetic Resonance in Medicine*, 42:1014–1018, 1999.

[4] C. Davatzikos, J.L. Prince, and R.N. Bryan. Image registration based on boundary mapping. *Medical Imaging, IEEE Transactions on*, 15(1):112–115, 1996.

[5] C. Dubois, L. Panicot-Dubois, G. Merrill-Skoloff, B. Furie, and B.C. Furie. Glycoprotein VI–dependent and–independent pathways of thrombus formation in vivo. *Blood*, 107(10):3902, 2006.

[6] T. Duza and I.H. Sarelius. Increase in endothelial cell ca2+ in response to mouse cremaster muscle contraction. *The Journal of Physiology*, 555(2):459–469, 2004.

[7] S. Falati, S. Patil, P.L. Gross, M. Stapleton, G. Merrill-Skoloff, N.E. Barrett, K.L. Pixton, H. Weiler, B. Cooley, D.K. Newman, et al. Platelet PECAM-1 inhibits thrombus formation in vivo. *Blood*, 107(2):535, 2006.

[8] M.W. Gaber, H. Yuan, J.T. Killmar, M.D. Naimark, M.F. Kiani, and T.E. Merchant. An intravital microscopy study of radiation-induced changes in permeability and leukocyte–endothelial cell interactions in the microvessels of the rat pia mater and cremaster muscle. *Brain Research Protocols*, 13(1):1–10, 2004.

[9] F.N.E. Gavins and B.E. Chatterjee. Intravital micro-scopy for the study of mouse microcirculation in anti-inflammatory drug research: focus on the mesentery and cremaster preparations. *J. Pharmacological and Toxicological Methods*, 49:1–14, 2004.

[10] A. Giachetti. Matching techniques to compute image motion. *Image and Vision Computing*, 18:247–260, 2000.

[11] S. Gupta, S. Akerman, A. van den Maagdenberg, PR Saxena, PJ Goadsby, and A. MaassenVanDenBrink. Intravital microscopy on a closed cranial window in mice: a model to study trigeminovascular mechanisms involved in migraine. *Cephalalgia*, 26(11):1294–1303, 2006.

[12] A.M. Iga, S. Sarkar, K.M. Sales, M.C. Winslet, and A.M. Seifalian. Quantitating Therapeutic Disruption of Tumor Blood Flow with Intravital Video Microscopy. *Cancer Research*, 66(24):11517, 2006.

[13] R.K. Jain, E.B. Brown, L.L. Munn, and D. Fukumura. Intravital Microscopy of Normal and Diseased Tissues in the Mouse. *Live Cell Imaging: A Laboratory Manual*, 2005.

[14] J.F. Krucker, G.L. LeCarpentier, J.B. Fowlkes, and P.L. Carson. Rapid elastic image registration for 3-D ultrasound. *Medical Imaging, IEEE Transactions on*, 21(11):1384–1394, 2002.

[15] B.D. Lucas and T. Kanade. An iterative image registration technique with an application to stereo vision. *International Joint Conference on Artificial Intelligence*, 81:674–679, 1981.

[16] F. Maes, A. Collignon, D. Vandermeulen, G. Marchal, and P. Suetens. Multimodality image registration by maximization of mutualinformation. *Medical Imaging, IEEE Transactions on*, 16(2):187–198, 1997.

[17] S. Magers and J.E. Faber. Real-time measurement of microvascular dimensions using digital cross-correlation image processing. *Journal of Vascular Research*, 29:241–247, 1992.

[18] J.A. Maintz and M.A. Viergever. A survey of medical image registration. *Medical Image Analysis*, 2(1):1–36, 1998.

[19] C.L. Murrant and I.H. Sarelius. Local and remote arteriolar dilations initiated by skeletal muscle contraction. *Am. J. Physiol. Heart Circ. Physiol.*, 279:H2285–H2294, 2000.

[20] J.W. Pluim, J.A. Maintz, and M.A. Viergever. Image registration by maximization of combined mutual information and gradient information. *Medical Imaging, IEEE Transactions on*, 19(8):809–814, 2000.

[21] T.A. Read, M. Farhadi, R. Bjerkvig, B.R. Olsen, A.M. Rokstad, P.C. Huszthy, and P. Vajkoczy. Intravital Microscopy Reveals Novel Antivascular and An-

titumor Effects of Endostatin Delivered Locally by Alginate-encapsulated Cells 1, 2001.

[22] S. Schmugge, W. Kamoun, J. Villalobos, M. Clemens, and M. Shin. Segmentation of vasculature for intravital microscopy using bridging vessel snake. *IEEE International Symposium on Biomedical Imaging*, pages 177–180, 2006.

[23] M. Sonka, W. Liang, and R.M. Lauer. Automated analysis of brachial ultrasound image sequences: early detection of cardiovascular disease via surrogates of endothelial function. *IEEE Transactions on Medical Imaging*, 21(10):1271–1279, October 2002.

[24] J. Tang and ST Acton. Vessel boundary tracking for intravital microscopy via multiscale gradient vector flow snakes. *Biomedical Engineering, IEEE Transactions on*, 51(2):316–324, 2004.

[25] K. Tyml, D. Anderson, D. Lidington, and H. Lakak. A new method for assessing arteriolar diameter and hemodynamic resistance using image analysis of vessel lumen. *American Journal of Physiology - Heart and Circulatory Physiology*, 284:1721–1728, May 2003.